Terminology for High-Speed Sampling-Oscilloscope Calibration

Dylan F. Williams, Tracy S. Clement, Paul D. Hale, and Andrew Dienstfrey

Abstract— **We discuss procedures for calibrating high-speed sampling oscilloscopes at the National Institute of Standards and Technology, and the terminology associated with those calibrations. The discussion clarifies not only the calibration procedures, but how to use the calibrations to perform traceable oscilloscope measurements.**

Index Terms—calibration, impedance mismatch, mismatch correction, sampling oscilloscope, terminology.

I. INTRODUCTION

CONVENTIONAL oscilloscopes are designed to non-invasively measure voltages inside operating electrical circuits. These oscilloscopes have a high input impedance, and typically have bandwidths of a few gigahertz. However, due to parasitics in the oscilloscope's input circuitry, at high frequencies, the oscilloscope's input impedance drops and its distortion increases, ultimately limiting the overall bandwidth of the oscilloscope.

High-speed sampling oscilloscopes circumvent these bandwidth limitations by embedding the sampling circuitry in a nominally 50 Ω transmission line terminated in a nominally 50 Ω load. Of course, this brings the input impedance of the oscilloscope down to a value near 50 Ω.

Unlike their conventional high-input-impedance counterparts, high-speed sampling oscilloscopes cannot be used to non-invasively measure voltages inside an operating circuit without external amplifiers designed to raise the input impedance presented to the circuit under test. Rather, these oscilloscopes are designed to be connected directly to the output port of a circuit, and to measure the voltage that the circuit generates across the oscilloscope's 50 Ω input impedance.

These high-speed oscilloscopes can be used to perform accurate mismatch-corrected measurements to frequencies of 100 GHz or higher, and offer a very convenient way of testing fast electrical components that are designed to operate in a 50 Ω electrical environment. In this paper we outline the procedures used at NIST for calibrating these nominally 50 Ω high-speed oscilloscopes [1] with calibrated photodiodes [2-6]
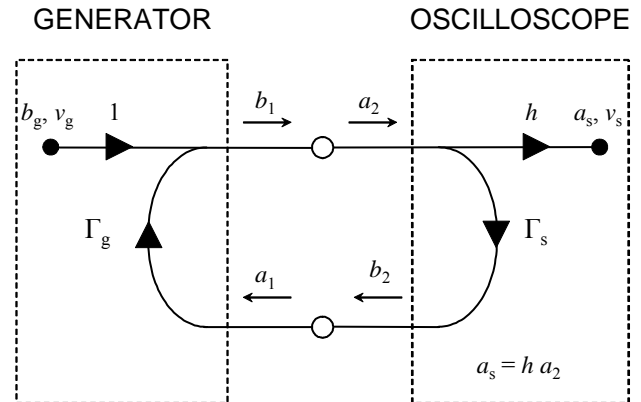

Fig. 1. Microwave flow diagram describing the propagation of signals between a generator and an oscilloscope. The generator on the left injects the signal b_g with no distortion, as indicated by the unity transfer function at the left of the flow diagram, into the circuit. The signal delivered to the oscilloscope is modified by the transfer function h, as well as being reflected multiple times by Γ_g and Γ_s.

and the terminology associated with those calibrations. We also explain how these calibrations can be used to obtain traceable mismatch-corrected oscilloscope measurements.

II. WAVE REPRESENTATION

It is common to use complex frequency-domain forward and backward wave amplitudes a and b normalized to a 50 Ω reference impedance in place of voltages and currents at microwave frequencies [7]. The complex wave amplitudes a and b are often referred to as phasors.

We use the "pseudowaves" of [7], which correspond to the conventional power-normalized forward and backward wave amplitudes with a reference impedance of 50 Ω [8]. These wave amplitudes have units of the square root of a watt, and are conventionally normalized so that the average power p transmitted across a reference plane is given by $p=\frac{1}{2}(|a|^2-|b|^2)$.[1]

By limiting ourselves to the characterization of signals with bandwidths below the cutoff frequency of the guiding structures we use, we are able to apply frequency-domain microwave mismatch corrections developed for linear time-

D. F. Williams, T. S. Clement, P. D. Hale, and A. Dienstfrey are with the National Institute of Standards and Technology, Boulder, CO 80305 USA (phone: 303-497-3138; e-mail: dylan@ boulder.nist.gov).

[1] Reference [1] uses a less common root-mean-square (RMS) normalization in which the power p is given by $p=|\underline{a}|^2-|\underline{b}|^2$, where $\underline{a}$ and $\underline{b}$ are the RMS pseudowaves of [1]. The RMS-normalized pseudowaves of [1] are related to those used here by $\underline{a}=a/\sqrt{2}$ and $\underline{b}=b/\sqrt{2}$.

invariant systems to the oscilloscope calibration problem. Figure 1 shows the microwave flow diagram describing the propagation of signals when a generator is connected directly to a high-speed sampling oscilloscope. This diagram is a simplification of the models developed in [9;10].

Strictly speaking, the diagram in Fig. 1 is applicable only to linear time-invariant circuits, and we must construct our experiments so that both requirements are met. In many cases the generator and oscilloscope impedances change during pulse generation and sampling, violating the linear time-invariant criteria. In addition, additive noise and imperfections in the oscilloscope timebase also violate the linear time-invariant criteria.

There are a number of strategies for mitigating these effects, some of which are listed below.

For the signal generator:
- The generator impedance can be made linear and time invariant with the addition of sufficient attenuation to the output of the generator.
- We can also achieve time invariance by adding a section of transmission line to the generator output that is long enough to prevent signals from being reflected back to the generator before its impedance has settled down to its steady state value. In this case, the generator's repetition rate must also be slow enough to ensure that all multiple reflections between the generator and the load have died down before the generator fires again and its impedance changes. However, adding a section of transmission line to the generator output does not ensure linearity of the generator's impedance.

For the oscilloscope:
- We correct for any time-base distortion and jitter in the oscilloscope time base.
- We average out any significant additive noise in the oscilloscope.
- We include a section of transmission line at the oscilloscope's input that is long enough to prevent signals reflected from the sampling gate when it closes from propagating back to the generator, being reflected, propagating back to the sampling gate, and being remeasured before the oscilloscope's sampling gate completely opens again.

When the circuit diagram of Fig. 1 can be applied, the generator on the left-hand-side of the diagram can be characterized by its forward-wave source amplitude b_g and its reflection coefficient Γ_g. This wave-based representation of the source is equivalent to the Thévenin-equivalent-circuit and Norton-equivalent-circuit representations commonly used to describe electrical sources at lower frequencies. References [2;8] present formulas for converting between this wave-based representation and Thévenin and Norton equivalent circuits.

In addition, the oscilloscope on the right-hand-side of Fig. 1 can be characterized by the Fourier transform h of its impulse response and by its reflection coefficient Γ_s.

For quasi-TEM guides with a suitable choice of voltage path, we can write the peak voltage v_g of the "forward voltage wave" associated with the wave amplitude b_g in Fig. 1 as [7]

$$v_g = \sqrt{50\,\Omega}\; b_g .\qquad(1)$$

The square root of 50 Ω in (1) converts the power-normalized wave amplitude b_g to a peak voltage. The voltage v_g is the peak voltage that the generator would generate across a perfect 50 Ω load. It can also be thought of as the voltage that the forward wave b_g would carry with it as it propagates down a perfect 50 Ω transmission line, and can be derived from Eq. (55) of [7] by setting the normalizing voltage v_0 in (55) real, the reference impedance Z_{ref} in (55) to 50 Ω, and the backward-wave amplitude b in (55) to zero.

Likewise, the relation between the peak voltage v_s that the oscilloscope measures and the wave a_s in Fig. 1 is given by

$$v_s = \sqrt{50\,\Omega}\; a_s .\qquad(2)$$

Finally, we would like to point out that the voltage v_g should not be confused with the total voltage at the generator's output port when the impedance of the load connected to the generator is not equal to 50 Ω. This is because the voltage at the output of the source depends on the impedance of the load connected to it. Measurement accuracy can be improved, particularly at high frequencies, by accounting for the imperfect impedances of the generator, oscilloscope, and device under test, with a "mismatch correction."

III. MISMATCH CORRECTION

We now solve for the wave amplitude a_2 in Fig. 1 created by the generator. The wave amplitudes at the generator's output port are related by [7;8]

$$b_1 = b_g + \Gamma_g\, a_1 ,\qquad(3)$$

while the wave amplitudes at the input of the oscilloscope are related by

$$b_2 = \Gamma_s\, a_2 .\qquad(4)$$

Since the generator and oscilloscope are connected directly together in Fig. 1, the voltages and currents are continuous across that junction, and $b_1=a_2$ and $a_1=b_2$. Thus, we can combine (3) and (4) to obtain [7;8;10]

$$a_2 = \frac{b_g}{1 - \Gamma_g \Gamma_s} .\qquad(5)$$

Finally, the oscilloscope measures the voltage v_s given by

$$v_s = \sqrt{50\,\Omega}\; a_s = \sqrt{50\,\Omega}\; h\,\frac{b_g}{1 - \Gamma_g \Gamma_s} = h\,\frac{v_g}{1 - \Gamma_g \Gamma_s} ,\qquad(6)$$

which can be rewritten as

$$h = \frac{b_\text{s}}{b_\text{g}}\left(1 - \Gamma_\text{g}\Gamma_\text{s}\right) = \frac{v_\text{s}}{v_\text{g}}\left(1 - \Gamma_\text{g}\Gamma_\text{s}\right). \tag{7}$$

We refer to h in (6) and (7) as the complex frequency response of the oscilloscope. This frequency response corresponds to a band-limited Fourier transform of the oscilloscope's impulse response, and accounts for the finite time it takes for the oscilloscope to respond to the signal delivered to it by the generator. It is equal to the ratio of the voltage v_s that the oscilloscope measures and the voltage $v_2 = \sqrt{50\,\Omega}\, a_2$ associated with the forward wave a_2 that the generator delivers to the oscilloscope.

IV. HIGH-SPEED OSCILLOSCOPE CALIBRATION

To calibrate a high-speed sampling oscilloscope, we determine the oscilloscope's complex frequency response h [1]. We can do this with a well characterized electrical impulse generator, such as a photodiode characterized on the NIST electro-optic sampling system [2-6], with known v_g and Γ_g. The procedure is conceptually quite straightforward. We first connect the photodiode to the oscilloscope, measure its output on the oscilloscope, correct for jitter, drift, and distortion in the oscilloscope's time base, and determine v_s. Then we use (7) to determine h from v_s and v_g.

Once h has been determined, we can use it to find the actual voltage v_DUT that a device under test would generate across a perfect 50 Ω load from the voltage $v_\text{DUT,raw}$ that the oscilloscope measures when connected to the device. We first correct for jitter, drift, and time-base distortion in the measurement of $v_\text{DUT,raw}$. Then we can calculate v_DUT from

$$v_\text{DUT} = v_\text{DUT, raw}\left(\frac{1 - \Gamma_\text{DUT}\,\Gamma_\text{s}}{h}\right), \tag{8}$$

where Γ_DUT is the reflection coefficient of the source.

V. CALIBRATION WITH AN ADAPTER

Finally, if we place an adapter with scattering parameters S_{ij} between the generator and the oscilloscope, the flow diagram shown in Fig. 2 applies. Then we can replace (5) with [8]

$$a_2 = \frac{b_\text{g}\,S_{21}}{1 - \Gamma_\text{g}S_{11} - \Gamma_\text{s}S_{22} - \Gamma_\text{g}\,\Gamma_\text{s}\left(S_{21}S_{12} - S_{11}S_{22}\right)}. \tag{9}$$

Now (7) becomes

$$h = \frac{v_\text{s}}{v_\text{g}}\left(\frac{1 - \Gamma_\text{g}S_{11} - \Gamma_\text{s}S_{22} - \Gamma_\text{g}\,\Gamma_\text{s}\left(S_{21}S_{12} - S_{11}S_{22}\right)}{S_{21}}\right). \tag{10}$$
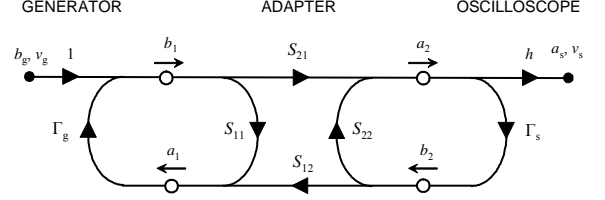

Fig. 2. Microwave flow diagram patterned after Fig. 1 describing the propagation of signals from a generator through an adapter to an oscilloscope.

This allows calibration through adapters and to different waveguide types and sizes.

VI. TRANSLATION TO THE TIME DOMAIN

The proceeding single-frequency analysis can be combined with a Fourier decomposition to solve more complex temporal problems. To solve these problems, we first decompose the temporal signal into its Fourier components, apply the preceding single-frequency analysis to each Fourier component, and then recompose the solution in the time domain from the single-frequency solutions. We consider two types of signals here, pulses with finite energy and periodic (repetitive) signals with infinite energy but finite power.

A. Pulse with finite energy

The total energy E in a signal $X(t)$ is given by $E = \int_{-\infty}^{\infty}|X(t)|^2\,\text{d}t$ [11].[2] If $X(t)$ has finite energy, we can represent $X(t)$ in the frequency domain with the complex continuous Fourier Transform $x(f)$ given by

$$x(f) = \int_{-\infty}^{\infty} X(t)\, e^{-j2\pi f t}\,\text{d}t, \tag{11}$$

where f is the frequency, t is the time, and j is the square root of -1 [11]. The inverse of (11) is

$$X(t) = \int_{-\infty}^{\infty} x(f)\, e^{j2\pi f t}\,\text{d}f. \tag{12}$$

The sign convention we use in the exponents of the integrals in (11) and (12) corresponds to the convention most commonly employed by the engineering community. If X has units of u,

---

[2] The energy E and power P we use here are defined in a mathematical sense in terms of $X(t)$. E and P should not be confused with the actual energy or power in the circuit, which must be ultimately determined with the inclusion of an appropriate reference impedance. We refer readers to [7] for a full discussion.

then we can see from (11) and (12) that its Fourier Transform x must have units of u multiplied by seconds. That is, x will have units u·s or u/Hz.

We often use the numerical Fourier Transform pair

$$x'_n = \frac{1}{N}\sum_{k=0}^{N-1} X'_k\, e^{-j(2\pi n/N)k} \qquad X'_k = \sum_{n=0}^{N-1} x'_n\, e^{j(2\pi k/N)n} \qquad (13)$$

to relate discretized versions of X and x [11]. Most signal-processing software packages support calculations of the sums in (13) directly or $1/\sqrt{N}$ scaled versions of those sums. These sums can also be very efficiently evaluated by the Fast Fourier Transform algorithm when N is equal to a power of 2.

If we set $X'_k = X(t_k)$ at the discrete times $t_k = k\,\Delta t$ in (13), then $x(f_n) \approx x'_n/\Delta f$ at the frequencies $f_n = n\,\Delta f$, where n and k are elements of $(0, 1, …, N\text{-}1)$ and Δt and Δf are chosen so that $N\,\Delta t\,\Delta f = 1$. Likewise, if we set $x'_n = x(f_n)\,\Delta f$, then $X(t_k) \approx X'_k$.

We can propagate $x(f)$ through any of the proceeding formulas (1) to (10) to construct new results. The positive Fourier coefficients of x propagate directly through any of the proceeding formulas (1) to (10) without change. Since all temporal signals are real, the negative-frequency Fourier coefficients are equal to the complex conjugate of the positive-frequency coefficients, and do not need to be calculated separately.

The energy spectral density S of $X(t)$ is defined as $S(f) = |x(f)|^2$ [11]. Parseval's theorem states that the total energy E in the signal can be computed in either domain:

$$E = \int_{-\infty}^{\infty} |X(t)|^2\, dt = \int_{-\infty}^{\infty} S(f)\, df = \int_{-\infty}^{\infty} |x(f)|^2\, df\ .$$ Note that $S(f)$ is defined over both the positive and negative frequencies, and that finding the total energy E in the signal $X(t)$ from its spectral density S requires integrating the energy spectral density over both the positive and negative frequencies.

Finally, if x corresponds to a power-normalized wave amplitude (i.e., a or b), then E is the actual energy in the circuit in joules. If x corresponds to a voltage or a current, we must scale E by the reference impedance to find the actual energy, as explained in [7].

B. Periodic signals with finite power

We use a slightly different representation for periodic (repetitive) functions with finite power. The total average power P carried by a periodic signal $X(t)$ is

$$P = \lim_{T\to\infty}\frac{1}{T}\int_{-T/2}^{T/2} X(t)\, dt\ ,$$ where T is the period of $X(t)$.[2] If $X(t)$ is a piece-wise continuous and bounded repetitive function of time satisfying $X(t) = X(t+T)$ with finite power P, we define the discrete Fourier representation of $X(t)$ in the frequency domain with

$$x_n = \frac{1}{T}\int_{t=0}^{T} X(t)\, e^{-j2\pi n\Delta f\, t}\, dt\ , \qquad (14)$$

where $T = N\,\Delta t = 1/\Delta f$ [11]. The inverse of (14) is

$$X(t) = \sum_{n=-\infty}^{\infty} x_n\, e^{j2\pi n\Delta f\, t}\ . \qquad (15)$$

Both X and the discrete Fourier coefficients x_n have the same units.

If we set $X'_k = X(t_k)$ at the discrete times $t_k = k\Delta t$ in (13), then $x_n \approx x'_n$. Likewise, if we set $x'_n = x_n$, then $X(t_k) \approx X'_k$.

The power spectral density $S_P(f)$ of X is a discrete function of f, and may be defined formally in terms of delta functions with

$$S_P(f) = \sum_{n=-\infty}^{\infty} |x_n|^2\, \delta(f - f_n)\ .$$ By Parseval's theorem, the total power P in the signal is

$$P = \lim_{T\to\infty}\frac{1}{T}\int_{-T/2}^{T/2} X(t)\, dt = \int_{-\infty}^{\infty} S_P(f)\, df = \sum_{n=-\infty}^{\infty} |x_n|^2$$ [11]. Here again, the sum must be performed over both the positive and negative frequencies.

C. Wave amplitudes, Fourier coefficients, and power

Microwave circuit theories, of which [7;8] are representative, are traditionally based on wave amplitudes a, b, v, etc. These wave amplitudes are also frequently referred to as phasors, are complex quantities, and are defined only at positive frequencies.

However, as we have already seen, temporal signals are typically decomposed into their Fourier coefficients, which are defined at both positive and negative frequencies. The positive-frequency Fourier coefficient is equal to one half of the corresponding wave amplitude, which is generally a complex number. Since the temporal signals are real, the Fourier coefficients at the negative frequencies are the conjugates of the Fourier coefficients at the positive frequencies, and we see that the information content in the two representations is the same.

An example illustrates the relationship between wave amplitudes and Fourier components. The actual temporal signal $X(t)$ associated with the wave amplitude a, for example, is $X(t) = \text{Re}(ae^{j2\pi f_0 t}) = |a|\cos(2\pi f_0 t + \arg(a))$. As stated earlier, the total average power P carried by this signal is

$$P = \lim_{T\to\infty}\frac{1}{T}\int_{-T/2}^{T/2} X(t)\, dt = \lim_{T\to\infty}\frac{1}{T}\int_{-T/2}^{T/2} |a|^2 \cos^2(2\pi f_0 t + \arg(a))\, dt = \tfrac{1}{2}|a|^2\ .$$

Setting $T = 1/f_0$, we see that the Fourier transform of $X(t) = |a|\cos(2\pi f_0 t + \arg(a)) = \frac{1}{2}(ae^{+j2\pi f_0} + ae^{-j2\pi f_0})$ is $x_1 = \frac{1}{2}a = \frac{1}{2}|a|e^{+j\arg(a)}$ and $x_{-1} = \frac{1}{2}a^* = \frac{1}{2}|a|e^{-j\arg(a)}$ [11]. We have now represented $X(t)$ with two Fourier coefficients x_1 and x_{-1} at the two frequencies $\pm f_0$, rather than a single wave amplitude a at frequency f_0. As before, the total power P in the signal is

$$P = \int_{-\infty}^{\infty} S_P(f)\, df = \sum_{n=-\infty}^{\infty} |x_n|^2 = |x_{-1}|^2 + |x_1|^2 = \left|\frac{a}{2}\right|^2 + \left|\frac{a}{2}\right|^2 = \tfrac{1}{2}|a|^2\ .$$

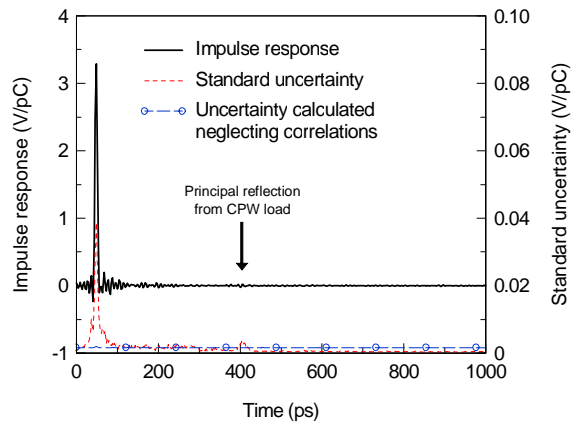However, to obtain this power, we had to integrate over both

Fig. 3. The impulse response of a photodiode calculated from frequency-domain data and its uncertainty determined both with and without correlations.

the positive frequency $+f_0$ and the negative frequency $-f_0$ at which the Fourier coefficients x_1 and x_{-1} are defined.

Finally, we note that microwave wave amplitudes are not typically defined at DC. The most logical definition at DC for a wave amplitude would be to set it equal to the Fourier coefficient at DC. However, this results in the confusing situation in which the wave amplitude at DC is equal to the Fourier coefficient at DC, but the wave amplitudes at other frequencies are equal to twice their corresponding Fourier coefficients. A better solution is to report the double-sided Fourier coefficients and power or energy spectral densities of temporal signals, which are consistently defined at DC, and use wave amplitudes only in the context of single-frequency sinusoidal analyses.

VII. Uncertainty Analyses

High-speed oscilloscope calibration with mismatch corrections inevitably requires use of a mix of temporal and frequency-domain measurements. The Fourier transform is a highly non-local transform, and correlations between errors cannot be ignored. This is because errors in one domain can either bunch up or spread out evenly in the other domain, depending on how they are correlated. For example, correlated ripples in the frequency domain may all bunch up at a single time, whereas uncorrelated noise in the frequency domain will be spread out evenly in the time domain.

The key to performing uncertainty analyses of high-speed oscilloscope and other systems based on both frequency-domain and temporal measurements is to keep track of the correlations of the errors as they are propagated from one domain to another during the analysis. At NIST, we represent the uncertainties in our high-speed oscilloscope calibrations in terms of covariance matrices, and use Jacobians to propagate our uncertainties through the analysis, as is done in [6]. This allows us to transform our uncertainties between the time and frequency domains.

Figure 3 illustrates the approach. The figure plots the point-by-point temporal impulse response of a photodiode measured on our electro-optic sampling system and calculated from its mismatch-corrected Fourier transform against the left axis of the figure. The figure also plots the uncertainty in this impulse response calculated two ways. The line with circles plots the standard uncertainty of the temporal impulse response calculated by ignoring the correlations in the frequency domain data. This results in a uniform uncertainty in time.

The dashed line shows the standard uncertainty calculated with the covariance matrix described in [6]. This formulation accounts for the correlations in the frequency-domain data when it maps the frequency-domain data into the time domain. This uncertainty is not uniform at all. First, the uncertainty in the measurement peaks near the maximum of the photodiode's impulse response. This component of the uncertainty is related to errors in calibrating the overall response of our electro-optic sampling system.

Less obvious is the smaller peak in uncertainty at 400 ps. The raw measurement of the photodiode's impulse response has a large reflection at that point, which is removed almost completely by the frequency-domain mismatch correction we employ. While the mismatch correction is very effective at eliminating this artifact of the measurement system near 400 ps, nevertheless, imperfections in the mismatch correction visibly raise the uncertainty there. This illustrates the utility of maintaining the correlations when calculating uncertainties of measurements based on a mix of temporal and frequency-domain quantities.

VIII. Conclusion

We have discussed some of the procedures used at the National Institute of Standards and Technology for determining the impulse response of high-speed photodiodes, and for calibrating high-speed oscilloscopes with those photodiodes. The measurements mix both temporal and frequency-domain measurements, which complicates both the terminology use to describe the measurements, and the uncertainty calculations associated with the measurements. Here we have endeavored to explain how we treat these complications in the measurements and calibrations.

References

[1] T. S. Clement, P. D. Hale, D. F. Williams, C. M. Wang, A. Dienstfrey, and D. A. Keenan, "Calibration of Sampling Oscilloscopes with High-Speed Photodiodes," *IEEE Trans. Microwave Theory Tech.*, Aug.6 A.D.

[2] D. F. Williams, P. D. Hale, T. S. Clement, and J. M. Morgan, "Mismatch corrections for electro-optic sampling systems," *Automatic RF Techniques Group Conference Digest*, vol. 56, pp. 141-145, Nov.2000.

[3]   D. F. Williams, P. D. Hale, T. S. Clement, and J. M. Morgan, "Calibrating electro-optic sampling systems," *IEEE MTT-S International Microwave Symposium Digest*, vol. 3, pp. 1527-1530, May2001.

[4]   T. S. Clement, P. D. Hale, D. F. Williams, and J. M. Morgan, "Calibrating photoreceiver response to 110 GHz," *15th Annual Meeting of the IEEE Lasers and Electro-Optics Society Confrence Digest*, pp. 877-878, Nov.2002.

[5]   D. F. Williams, P. D. Hale, T. S. Clement, and C. M. Wang, "Uncertainty of the NIST electrooptic sampling system," *NIST Tech. Note 1535*, Dec.2004.

[6]   D. F. Williams, A. Lewandowski, T. S. Clement, C. M. Wang, P. D. Hale, J. M. Morgan, D. A. Keenan, and A. Dienstfrey, "Covariance-Based Uncertainty Analysis of the NIST Electro-optic Sampling System," *IEEE Trans. Microwave Theory Tech.*, vol. 54, no. 1, pp. 481-491, Jan.2006.

[7]   R. B. Marks and D. F. Williams, "A general waveguide circuit theory," *J. Res. Nat. Instit. Standards and Technol.*, vol. 97, no. 5, pp. 533-562, 1992.

[8]   D. M. Kerns and R. W. Beatty, *Basic theory of waveguide junctions and introductory microwave network analysis*, 1 ed. Oxford, New York: Pergamon Press, 1967.

[9]   J. Verspecht and K. Rush, "Individual characterization of broadband sampling oscilloscopes with a nose-to-nose calibration procedure," *IEEE Trans. Instum. Meas.*, vol. 43, no. 2, pp. 347-354, Apr.1994.

[10]   D. C. DeGroot, P. D. Hale, M. Vanden Bossche, F. Verbeyst, and J. Verspecht, "Analysis of interconnection networks and mismatch in the nose-to-nose calibration," *Automatic RF Techniques Group Conference Digest*, vol. 55, pp. 116-121, June2000.

[11]   F. G. Stremler, *Introduction to communication systems*, 2 ed. Reading, MA: Addison-Wesley Publishing Company, 1982.